Synthesizing Virtual Measurements of Moving Sound Sources in the Atmospheric Boundary Layer

Dorothea Lincke, Reto Pieren

Empa, Swiss Federal Laboratories for Materials Science and Technology, 8600 Dübendorf, Switzerland

Correspondence to: dorothea.lincke@empa.ch

Introduction

Exposure to aircraft noise has a significant impact on humans, such as annoyance, sleep disorders, cardiovascular diseases, and impaired cognitive development of children [1]. Therefore, noise impact assessments and noise control at the source are important aspects of the design of new aircraft.

The design process of low-noise aircraft can be supported with auralization [2]. Auralization is a technique of rendering numerical data audible. Thus, design changes leading to changing sound emissions, can be evaluated auditorily before the aircraft has been built. Further, laboratory tests for noise impact assessments can be conducted with controllable, synthetized sound samples instead of recorded sound samples. For these applications of auralization, the synthesized sound samples should be perceived as plausible.

In order to render plausible aircraft auralizations, multiple propagation phenomena have to be considered, such as geometrical spreading, air absorption, Doppler effect, and reflections from the ground. The ground-reflected sound is often modeled by introducing an image source.

Additionally, atmospheric turbulence causes characteristic fluctuations of sound amplitude and phase because of turbulent fluctuations of temperature and wind velocity along the sound propagation path. If the receiver is located at a height $h_r > 0\,\mathrm{m}$ above the ground, phase fluctuations decrease the coherence between direct and ground-reflected sound waves, thus changing the ground interference pattern at the receiver position. Because these turbulence-induced effects are typically not considered in aircraft auralizations, they are considered less plausible compared to sound recordings.

The ongoing international research project *LION - Localization and identification of moving noise sources* has the objective to enhance the reliability of microphone array methods for moving sound sources such as aircraft and rail vehicles. Microphone array methods are broadly used in industry and research for the purpose of localizing static sound sources [3]. In case of moving sound sources, results of microphone array measurements suffer from the uncertainties induced by propagation effects in the atmosphere, varying ground reflection properties, short measurement times and the Doppler frequency shift which is caused by the source's movement.

Synthesizing virtual measurements is a considerable asset to the development and validation of microphone setups and source localization methods like beamforming. Unlike measured microphone signals, synthesized signals allow for full control of sound source characteristics and the trajectory of the movement. Virtual test cases will allow to investigate the sensitivity of microphone array methods to properties of the propagation path like ground properties and varying atmospheric conditions and will facilitate improvements of microphone array methods.

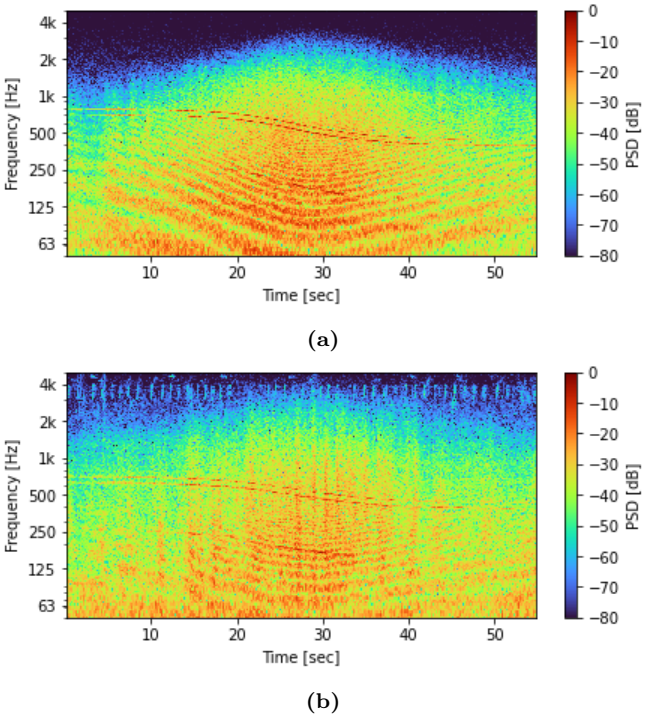

Figure 1: Aircraft flyover of identical Airbus A320 during approach at approx. 700 m height. 1a is recorded in the evening, stable atmosphere with low turbulence. 1b is recorded in the morning, near-neutral atmosphere, strong wind and strong atmospheric turbulence.

Turbulence effects in aircraft flyover field measurements

Figure 1 shows two flyover measurements of an Airbus A320 approaching Zurich airport at about 700 m height above ground. The aircraft and the recording position (10 m height) are identical in both measurements, whereas the recording day and daytime are different. The measurement in Fig. 1a was taken in the evening with a stable atmosphere and weak wind conditions. A stable atmosphere has low atmospheric turbulence as the temperature stratification suppresses the vertical wind

velocity component. The spectrogram in Fig. 1b shows a recording in the morning with strong wind and a near-neutral atmosphere, leading to strong atmospheric turbulence. The periodic pattern above 3 kHz is caused by birds chirping.

The following propagation effects are visible in both spectrograms: the Doppler frequency shift of the two wing cavity tones at about 500 Hz to 700 Hz; the effect of the distance-dependent atmospheric absorption for frequencies above 1 kHz; and the comb-filter effect due to the interference of the direct and the ground reflected sound.

Unlike Fig. 1a, Fig. 1b shows signs of strong atmospheric turbulence. Firstly, it shows broadband temporal level fluctuations, which are well audible in the recording. Secondly, the ground interference pattern is considerably weaker as atmospheric turbulence leads to partly randomized acoustic phases and therefore a coherence loss between different sound propagation paths. Additionally, the ground interference pattern is less smooth over time.

Accounting for atmospheric turbulence

Methods in outdoor sound propagation make often use of the effective sound speed approximation in order to account for advection of sound by wind:

$$c_{\text{eff}} = c + \mathbf{u}\vec{e}, \tag{1}$$

where c is the speed of sound, $\mathbf{u}$ is the wind velocity vector, and $\vec{e}$ is a unit vector in the direction of sound propagation. Turbulent fluctuations of wind velocity and temperature lead to fluctuations of the effective sound speed and consequently to fluctuations of the acoustic refractive index $n = \frac{c_0}{c}$, where c_0 is the sound speed at a reference temperature T_0. These fluctuations lead to fluctuations of sound amplitude and acoustic phase.

In the following, we will propose three strategies for studying the influence of atmospheric turbulence on sound propagation.

Generating fields of random fluctuations of $\mathbf{u}$ and T allows to study numerically the sound propagation in these fields. Common numerical methods are raytracing and finite-difference time-domain (FDTD) methods. Figure 2 shows an example of a synthesized scalar random field for temperature fluctuations superposed with a vertical temperature profile $T(z)$. The simulation is based on a Quasi-wavelet method [4] and represents the situation of an unstable atmosphere.

Instead of generating random fields of $\mathbf{u}$ and T, which can be computationally expensive, analytical solutions of the turbulence induced complex sound pressure fluctuations can be used. Ostashev and Wilson have developed a rigorous description based on the narrow-angle parabolic equation. The method describes variances and correlation functions of log-amplitude and phase fluctuations, as well as statistical moments of the sound field. This approach is time efficient, as the computation of random fields and sound propagation is not required. Therefore, the approach is more flexible to account for different meteorological regimes. These analytical descriptions are still subject to ongoing research and have not been fully validated by field measurements.

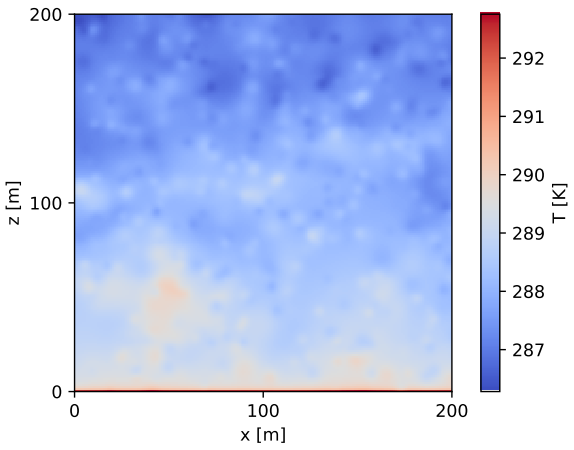

Figure 2: Scalar random field of temperature fluctuations in an unstable atmosphere.

The third strategy is to carry out field measurements and determine empirical parameters. Acoustic measurements can be complemented by meteorological measurements of mean temperature and wind and by turbulence measurements with an ultrasonic anemometer.

In the following, we will focus on the second strategy and present an approach to account for turbulence induced coherence loss in ground effect.

Coherence loss in ground effect

We consider a moving sound source at height h_s above an idealized infinite impedance plane, and a receiver at height h_r. To determine the sound pressure at the receiver, the relative phase between direct and ground reflected sound waves must be taken into account. The ensemble-averaged, mean-squared sound pressure $\langle pp^* \rangle$ at a receiver position can be described by [5]:

$$\langle pp^* \rangle = \frac{1}{r_{\text{d}}^2} + \frac{|Q|^2}{r_{\text{r}}^2} + \frac{2|Q|C_{\text{coh}}}{r_{\text{d}} r_{\text{r}}} \cos\left[k\left(r_{\text{d}} - r_{\text{r}}\right) + \phi\right] \tag{2}$$

where r_d and r_r are the lengths of the direct and ground reflected sound propagation paths, $Q = |Q|e^{j\phi}$ spherical wave reflection coefficient, k acoustic wave number. The coherence factor C_{coh} represents the effect of atmospheric turbulence on the relative phase between direct and ground-reflected sound waves. In [5], the coherence factor is based on a Gaussian correlation function of the refractive index fluctuations as proposed by Daigle [6]. The refractive index fluctuations describe the refraction of sound waves caused by effective sound speed fluctuations.

Ostashev and Wilson presented later a new derivation of the coherence factor C_{coh} [4]. Here, C_{coh} is based on the parabolic equation method and the von Kármán turbulence spectrum. Vertical profiles of wind velocity $\mathbf{u}$ and temperature T are described by Monin-Obukhov similarity theory (MOST) and mixed-layer similarity theory. The turbulent fluxes are parametrized with turbulence

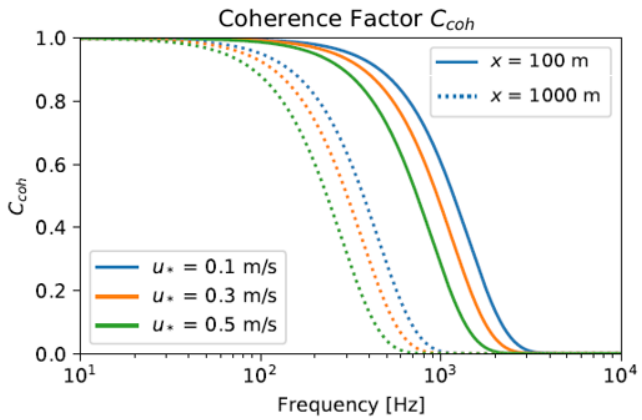

Figure 3: Dependence of coherence factor C_{coh} on frequency f, friction velocity u_*, and distance x.

scaling parameters.

The appropriate choice of the turbulence scaling parameters friction velocity u_*, surface heat flux Q_H, and Obukhov length L_o allows to account for different meteorological conditions. Friction velocity u_* describes the shear produced kinetic turbulence. The surface heat flux Q_H accounts for turbulent transport of heat either upwards, when the surface is warmer than the air, or downwards if the surface is cooler than the air. The Obukhov length L_o describes the height below which shear produced turbulence dominates. It is an indicator for the atmospheric stability. These parameters can be locally determined with an ultrasonic anemometer. In contrast, the earlier approach of Daigle [6] is based on the fluctuations of the index of refraction $\langle \mu^2 \rangle$. The value for $\langle \mu^2 \rangle$ is usually taken from literature, as it is more complex to determine. Further, Daigle neglected the influence of the vector character of the wind velocity fluctuations.

Figure 3 shows the coherence factor C_{coh} calculated with Ostashev and Wilson's model. The coherence factor decreases with frequency and for increasing distance x and friction velocity u_*. Likewise, a stronger surface heat flux Q_H leads to a moderate decrease of coherence. $C_{\mathrm{coh}} = 1$ corresponds to no phase shift between direct and ground reflected sound waves leading to a strong ground effect pattern due to constructive and destructive interference. $C_{\mathrm{coh}} = 0$ accounts for fully randomized phases and thus merely energetic summation of the direct and ground reflected propagation path.

Both models for C_{coh} are exponential functions of f^2 thus leading to qualitatively identical frequency dependencies, if the meteorological parameters are chosen appropriately. However, the explicit dependence on u_* and Q_H makes the latter model more flexible and applicable as complement to field measurements.

Decorrelation filter

We use the coherence factor to design a time-varying and frequency-dependent decorrelation filter based on [7]. This all-pass filter is energy-neutral. The design

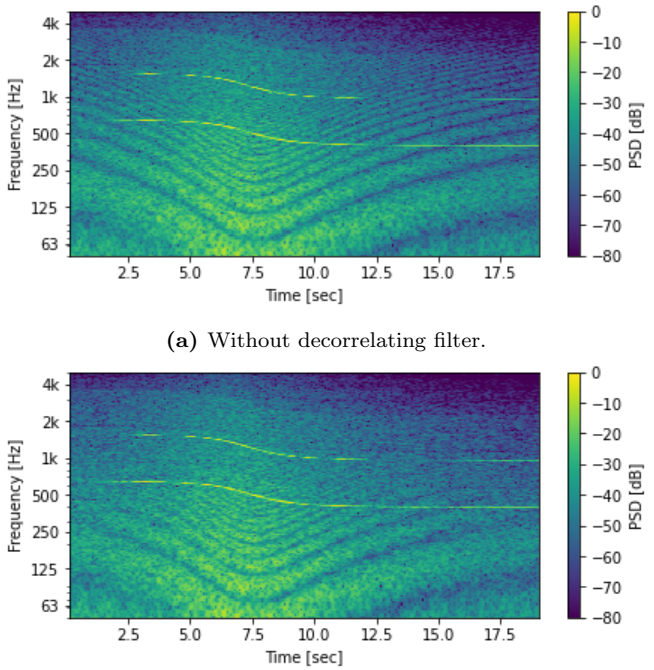

(a) Without decorrelating filter.

(b) With application of decorrelating filter.

Figure 4: Spectrograms of auralized fly-over before and after application of the decorrelating filter. Virtual microphone position: $x = 800\,\mathrm{m}, y = 0\,\mathrm{m}, z = 4\,\mathrm{m}$. Source moves at constant speed 250 km/h on straight line from $x = 0\,\mathrm{m}$ to $x = 1600\,\mathrm{m}$; $y = 50\,\mathrm{m}, z = 150\,\mathrm{m}$.

frequency response of the filter is written as

$$B(f) = e^{-j\beta(f)\varphi(f)} \tag{3}$$

The phase response of the filter contains a random phase distribution of $\varphi \sim U(-\pi, \pi)$. The phase scaling coefficient $\beta(f)$ incorporates the frequency dependent coherence factor $C_{\mathrm{coh}}(f)$ and is limited to $0 \leq \beta \leq 1$.

The filter is realized with an FIR filter of 80 ms length which is updated every 200 ms to the new position of the moving sound source. Consecutive time frames are cross-faded to suppress discontinuities. The application of the filter to the ground-reflected sound simulates a partial coherence loss between direct and ground-reflected sound and thus less pronounced ground effect patterns, particularly at high frequencies and large distances.

Application example

Figures 4a and 4b show the spectrograms of the auralized flyover before and after the proposed decorrelating filtering. The auralization reproduces the following scenario. A monopole sound source moves at 250 km/h along a straight trajectory at 100 m height from $x = 0\,\mathrm{m}$ to $x = 1600\,\mathrm{m}$ in the $y = 0$ plane. The source signal is colored noise with added sinusoidal components at 500 Hz and 1200 Hz. The virtual microphone is placed at $x = 800\,\mathrm{m}, y = 50\,\mathrm{m}, z = 4\,\mathrm{m}$.

Figure 4a shows the spectrogram of the auralization for a homogeneous atmosphere with temperature $T = 15\,^{\circ}\mathrm{C}$, relative humidity $q = 70\%$, no wind or turbulence and grassy ground with airflow resistivity $\sigma = 200\,\mathrm{kPa} \cdot \mathrm{s/m^2}$.

The simulation is based on [8]. The air absorption calculation follows the ISO standard 9613-1 [9]. Ground impedance is calculated with the Miki model [10].

Figure 4b shows the same simulation after additional application of the decorrelation filter. The coherence factor C_{coh} is determined for a turbulent atmosphere characterized by friction velocity $u^* = 0.3\,\mathrm{m/s}$, surface sensible heat flux $Q_H = 200\,\mathrm{W/m^2}$, and boundary layer height $z_i = 1\,\mathrm{km}$. These values correspond to a sunny day with medium wind speed. The interference pattern in Figure 4b is considerably weaker than in Figure 4a. This is especially noticeable for the the first seconds, in which no interference is visible in frequencies above 200 Hz. The distance dependence of C_{coh} results in stronger constructive and destructive interference when the moving source is closer to the virtual microphone. The difference between the signals in Figure 4a and 4b is well audible.

Conclusion

Atmospheric turbulence affects long-range sound propagation outdoors. These turbulence effects are of relevance in the context of measurements of moving sound sources using microphone arrays or in auralization of environmental noise sources such as aircraft or wind farms. Atmospheric turbulence should be considered in synthesized measurements and auralizations to achieve a high degree of accuracy and plausibility, respectively.

Different approaches for accounting for atmospheric turbulence in auralization of outdoor sound propagation were discussed in this paper. As an example, we developed a strategy to account for coherence loss between direct and ground reflected sound. The coherence loss is described by the coherence factor as derived by Ostashev and Wilson. The atmosphere is represented by Monin-Obukhov and mixed-layer similarity theory where turbulence fluxes are parameterized by the scaling parameters friction velocity, surface heat flux, and Obukhov length. The computation of the coherence factor is based on the von Kármán spectrum. Different meteorological regimes can be represented by the appropriate choice of the turbulence scaling parameters. For a given coherence factor an energy-neutral, decorrelation filter was designed to simulate coherence loss.

The application of the proposed filter to the ground reflected path leads to a clear reduction of the interference pattern after summation of the direct and the ground reflected path. This difference is well audible.

The work of Ostashev and Wilson is a promising basis for further filter design. Nevertheless, the theory and the resulting auralization will require validation by field measurements as well as possible complementations and adaptations.

Two extensions to the auralization model are already in preparation. First, a filter accounting for level fluctuations caused by atmospheric turbulence will be implemented. Second, the relation between multiple distributed receivers will be considered by incorporating the mutual coherence of separate sound propagation paths. With this extension, it will be possible to synthesize realistic microphone array signals including the effect of atmospheric turbulence.

The findings of this research will be valuable beyond the LION project for studying environmental noise impact. So far, noise exposure is usually described by time-averaged levels. These measures do not reflect the sound's dynamic character and peak noise levels. Further, auralization allows to include perception-based evaluations of virtual flyovers into the design processes of future low-noise transportation technologies [8].

Funding

This research was supported by the international research project Localization and Identification Of moving Noise sources (LION) in which the Swiss contribution was funded by the Swiss National Science Foundation (SNSF) by grant No. 185530. This work is also part of the research project Aircraft noise Reduction Technologies and related Environmental iMpact (ARTEM), which has received funding from the European Union's Horizon 2020 research and innovation program under grant agreement No. 769350.

References

[1] World Health Organization. Regional Office for. *Environmental noise guidelines for the European Region*. World Health Organization. Regional Office for Europe, Copenhagen, 2018.

[2] Rizzi and Sahai. Auralization of air vehicle noise for community noise assessment. *CEAS Aeronautical Journal*, 10(1):313–334, 2019.

[3] Merino-Martínez, Sijtsma, Snellen, Ahlefeldt, Antoni, Bahr, Blacodon, Ernst, Finez, Funke, Geyer, Haxter, Herold, Huang, Humphreys, Leclère, Malgoezar, Michel, Padois, Pereira, Picard, Sarradj, Siller, Simons, and Spehr. A review of acoustic imaging methods using phased microphone arrays. *CEAS Aeronautical Journal*, 10(1):197–230, 2019.

[4] Ostashev and Wilson. *Acoustics in Moving Inhomogeneous Media*. CRC Press, Taylor & Francis Group, Boca Raton, 2nd edition, 2016.

[5] Clifford and Lataitis. Turbulence effects on acoustic wave propagation over a smooth surface. *The Journal of the Acoustical Society of America*, 73(5):1545–1550, 1983.

[6] Daigle, Piercy, and Embleton. Effects of atmospheric turbulence on the interference of sound waves near a hard boundary. *The Journal of the Acoustical Society of America*, 64(2):622–630, 1978.

[7] Kendall. The decorrelation of audio signals and its impact on spatial imagery. *Computer Music Journal*, 19(4):71, 1995.

[8] Pieren, Bertsch, Lauper, and Schäffer. Improving future low-noise aircraft technologies using experimental perception-based evaluation of synthetic flyovers. *Science of The Total Environment*, 692:68–81, 2019.

[9] International Organization of Standardization. ISO 9613-1: Acoustics – Attenuation of sound during propagation outdoors - Part 1: Calculation of the absorption of sound by the atmosphere, 1993.

[10] Miki. Acoustical properties of porous materials. modifications of delany-bazley models. *Journal of the Acoustical Society of Japan (E)*, 11(1):19–24, 1990.